

Remote Sensing Image Recognition and Classification Based on Complex Networks

YUCHEN WANG^{1,2}, GUANGDONG HUANG¹, AND ZONGWEI WANG^{2,3}

¹College of Mathematics and Physics, China University of Geosciences, Beijing 100083, China

²Key Laboratory of Land satellite Remote sensing Application, Ministry of Natural Resources of the People's Republic of China, Beijing 100083, China

³Jiangsu Province Surveying and Mapping Engineering Institute, Nanjing 210000, China

Corresponding author: Guangdong Huang (gdhuang@cugb.edu.cn)

This work was supported in part by the Key Laboratory of Land Satellite Remote Sensing Application, Ministry of Natural Resources of the People's Republic of China under Grant KLSMNR-K202207, and by the Natural Resources Dynamic Monitoring Project under Grant NTGC0091304.

ABSTRACT This paper presents a complex network-based feature extraction method designed to address the diversity and complexity of remote sensing images to enhance classification accuracy. The proposed method comprises three key components: (1) texture analysis of remote sensing images in various settings, showing differences in the distribution of edge weights within the first regular network according to texture categories, where rougher textures require higher thresholds to form the network; (2) feature extraction through a combination of static statistics and threshold evolution within the complex network, leading to the creation of a robust network model; (3) a convolutional neural network is utilized to classify and predict the processed remote sensing images, and the results are compared to the original image categorization. The experimental results demonstrate that images processed via complex networks exhibit higher classification accuracy. This method performs superior classification and provides new insights into remote sensing image classification and recognition.

INDEX TERMS Complex networks, image classification, remote sensing, texture analysis.

I. INTRODUCTION

China's remote sensing satellite technology for Earth observation has developed rapidly, and it has the ability to acquire remote sensing data independently and independently, ensuring the quantity and quality of data. Researchers are concentrating on more successfully mining data from high-quality remote sensing images and extracting their properties to support diverse applications. However, the complexity and variety of imaging scenes in remote sensing images present significant obstacles. Seasons, weather, latitude, and human influences all easily influence these images, creating diverse and intricate settings. Different natural and artificial landscapes, such as farms, rivers, forests, and buildings, are a sign of diversification. The notable distinctions between features within the same kind of scene and the similarities between features in other scenes demonstrate the scene's complexity. Consequently, one critical challenge is appropriately using the information that may be extracted from remote sensing images of various scenarios.

To address this challenge, numerous studies at this stage utilize deep learning techniques and rely on massive datasets to train models for remote sensing image

recognition and classification. In the realm of scene classification of remote sensing images based on convolutional neural networks(CNNs), Gong Cheng et al. conducted a comparison test on the NWPU-RESISC45 dataset, concluding that CNN-based scene classification methods significantly outperform traditional methods[1]. Weijia Li et al. employed a CNN to classify and recognize oil palm trees in a high-resolution remote sensing image dataset, achieving an accuracy rate of 96% [2]. Zhong Ma et al. designed a deep convolutional neural network (DCNN) incorporating an Inception module for satellite image classification[3]. They proposed a hyper-parameter optimization method based on a genetic algorithm, significantly improving classification accuracy. Zhou Z et al. introduced a ResNet-TP network, a two-way residual network, enhancing the network's feature extraction capability[4]. Sun et al. developed a multilevel convolutional pyramid semantic fusion structure, which improved the feature extraction capability of CNNs for multi-scale ground objects and significantly enhanced classification performance[5]. Fan et al. proposed a CNN model that adaptively focuses on crucial information in remote sensing images while ignoring redundant

information to achieve optimal classification performance[6]. Qun Liu et al. presented a new framework for remote sensing image classification, combining CNNs and manual features to design a six-layer CNN, incorporating a feature fusion layer to input manual features, thereby improving classification performance through feature fusion[7]. All these studies enhance the accuracy of remote sensing image classification by advancing deep learning algorithms.

Recently, academics have been paying more attention to using complex networks in image processing. In contrast to deep learning, complex networks are based on graph theory, which views pixels as vertices and the lines connecting them as either directed or undirected edges. More stability and robust noise tolerance can be obtained by representing images with complex networks, which improves image recognition performance. André Ricardo Backes et al. introduced a method for constructing shape descriptor signatures using a small-world complex network, demonstrating high efficiency, robustness, noise tolerance, and invariance to scale and rotation[8]. Wesley Nunes Gonçalves et al. proposed a graph-based approach for face recognition, modeling face images as graphs and extracting feature vectors using a complex network approach[9]. Their experiments showed that this method is rotationally invariant and outperforms other algorithms. Lijian Zhou et al. developed a hierarchical palmprint feature extraction and recognition method based on multi-wavelet and complex networks, effectively reducing redundant information and enhancing key points of central lines and wrinkles with notable robustness[10]. Ma Huang et al. proposed a novel image classification method combining complex networks and CNNs, utilizing the topological invariance of complex networks to mitigate the effects of rotation, translation, and scaling, achieving high classification accuracy and unique network features[11]. These studies indicate that complex networks exhibit excellent stability and robustness in image representation, suggesting their potential application in addressing the diversity and complexity of remote sensing images.

A complex network can extract the feature information that most closely matches the remote sensing image in the current scene before a convolutional neural network classifies the image. This will allow the complexity of the features in the remote sensing image to be better addressed and the image to be classified more effectively. Texture analysis is a crucial component of computer vision and image processing applications. Its primary goal is to model and analyze images to extract information, duplicate the human visual system, and enable the in-depth study of their data. Because diverse scenes in remote sensing images contain different texture information, texture plays a more significant role in classifying those images. With the rich feature information in remote sensing images, texture analysis can discern and identify the salient characteristics

of various features in various scenarios. For instance, features like farms and forests may all be identified with the help of texture analysis.

Therefore, this paper combines deep learning with complex networks to identify and categorize remote sensing images with different textures. Initially, complex networks are utilized to comprehensively extract feature information from remote sensing images by analyzing their textures across different categories. Subsequently, the processed images are classified and predicted using deep learning. In particular, we use the Eurosat for experimental validation and GoogleNet to categorize and predict remote sensing images processed by complex networks. This strategy aims to classify and apply remote sensing images with greater accuracy. The paper proposes an approach that attempts to provide new concepts and methods for feature extraction of remote sensing images in various settings and improve classification accuracy.

II. Methods

A. Complex Networks

A network is a collection of nodes (or vertices) and edges (or links) connecting those nodes. In a network, nodes represent various entities, such as individuals, objects, or events, while edges represent relationships or interactions between nodes. These relationships can be direct connections or interactions that reflect some kind of link between nodes. *Complex networks* are a particular type characterized by their complexity and unique properties. Compared to traditionally essential networks, complex networks usually feature more varied connection patterns and complicated topologies. In complex networks, the nodes and edges can have a wide range of characteristics and interactions; they frequently show dynamics, self-organization, and nonlinearity. Complex networks are essential and helpful in many real-world applications because of their common characteristics, which include small-worldness, scale-free qualities, and community structure.

In many natural and social systems, such as social networks, biological networks, and information networks, Complex Networks have been found. The Random Network Model and the Small-World Network Model are two examples of common complex networks.

Erdős and Rényi proposed the Random Network Model, which is frequently referred to as the Erdős-Rényi model. According to this model, every pair of nodes is connected with an equal probability, which implies that each edge's existence in the network is independent and random. As an example of the random network model, let us say a class of students wishes to make friends on a social media site. To begin simulating their friendships, we assume every student is a node in the random network model. The connection probability is then set to $P = 0.2$, which indicates a 20% likelihood of friendship between every pair of students. Ultimately, we randomly chose each student couple and used

this 20% likelihood to determine whether or not the students become friends. Most students in this simulation will have roughly the same number of friends; however, some may have unusually few or many friends because of randomization. This network of randomly formed friendships demonstrates a stochastic network concept.

Despite its simplicity, the Internet, biological networks, social networks, and other real-world networks can all be better understood and analyzed thanks to the stochastic network model. It gives a basic framework for comprehending intricate networks. We can better understand the structure and characteristics of different networks by contrasting the stochastic network model with more intricate models, such as scale-free networks and small-world networks.

Features of regular and random networks are combined in Watts and Strogatz's Small-World Network Model (SWMN). Two steps are involved in building the SWMN: First, every node is connected to its k nearest neighbors in a regular cyclic network. Each node in a network with N nodes is connected to the k nearest neighbors, resulting in a regular network that is locally connected. The network's edges are then rejoined with a given probability P . To make a reconnection, one end of an edge is connected at random, rather than with its closest neighbor, to another node in the network. Watts and Strogatz found that the network shows small-world features where the average path length L decreases rapidly. At the same time, the clustering coefficient C remains high as the reconnection probability P steadily increases from 0. Numerous real-world networks, including social and biological networks, are well-modeled by this structure. The following formulas calculate the clustering coefficient C and average path length L .

$$C = \frac{1}{N} \sum_{i=1}^N C_i \quad \text{where } C_i = \frac{2E_i}{k_i(k_i - 1)} \quad (1)$$

$$L = \frac{1}{\frac{N(N-1)}{2}} \sum_{i < j} d_{ij} \quad (2)$$

Combining the characteristics of random and regular networks, small-world network models accurately depict a wide range of complex network architectures found in the actual world. In social networks, for instance, many people are connected, either directly or indirectly, and even if they live far apart, they may typically connect through a small number of intermediaries. This reflects the "six degrees of separation" phenomenon, according to which there might be up to six acquaintances separating any two persons on Earth. In conclusion, the small-world network model is valuable for researching network features since it maintains a high clustering coefficient and accomplishes a short average path length using a straightforward reconnection process.

Complex networks are essential in biological networks, such as the study of protein interaction networks, gene regulatory networks, and metabolic networks, in addition to their uses in social networks. Additionally, they are necessary for the

modeling and analysis of transportation networks, including public transportation, aircraft, and road networks. Complex networks are also essential in ecological networks for studying food webs and ecological interactions and in power networks for analyzing and optimizing power systems. These numerous applications highlight how flexible and valuable complex network theory is for comprehending and improving real-world systems.

B. Indicators for Categorical Assessment

In machine learning and data mining, evaluation metrics like accuracy, precision, recall, and F1-score are frequently employed to assess the effectiveness of categorization models. These metrics work together to give a complete picture of a model's performance. We will introduce each of these four assessment metrics and their definitions and calculations in the following.

Accuracy is the ratio of the number of samples correctly predicted by the model to the total number of samples. It is defined as follows:

$$\text{Accuracy} = \frac{TP + TN}{TP + TN + FP + FN} \quad (3)$$

where TP (True Positive) denotes the number of samples that are actually positive and predicted to be positive; TN (True Negative) denotes the number of samples that are actually negative and predicted to be negative; FP (False Positive) denotes the number of samples that are actually negative but predicted to be positive; and FN (False Negative) denotes the number of samples that are actually positive but predicted to be negative.

Precision is the proportion of samples predicted to be positive that are actually positive. In other words, it assesses the degree to which the model's positive predictions come true, indicating how many of the samples that are labeled as positive are.

$$\text{Precision} = \frac{TP}{TP + FP} \quad (4)$$

Recall is the proportion of samples that are actually positive and are correctly predicted as positive by the model. It indicates how many genuinely positive samples are included in the model's predictions by calculating the model's accuracy in identifying all positive samples.

$$\text{Recall} = \frac{TP}{TP + FN} \quad (5)$$

The F1 value (F1-score) is the harmonic mean of precision and recall, effectively combining both metrics to evaluate the model's performance. It is a reliable statistic that is especially helpful for evaluating model performance in situations where sample categories are unbalanced.

$$F1 - \text{score} = 2 \times \frac{\text{Precision} \times \text{Recall}}{\text{Precision} + \text{Recall}} \quad (6)$$

III. Application Cases

A. Complex Network-Based Texture Feature Extraction for Remote Sensing Images

1) DATASETS

This paper uses the 64×64 image pixel size from the Eurosat for memory and computational speed considerations. It confirms that the complex network may successfully increase the classification accuracy of remote sensing images. Based on Sentinel-2 satellite photos, the Eurosat is widely used for land cover detection and classification experiments. With 27,000 annotated and georeferenced images, it spans 13 spectral bands and includes 10 categories, such as Residential and Industrial Buildings. As seen in Figure 1, each category has roughly 2,000–3,000 remote sensing images, each with a resolution of 64 by 64 pixels.

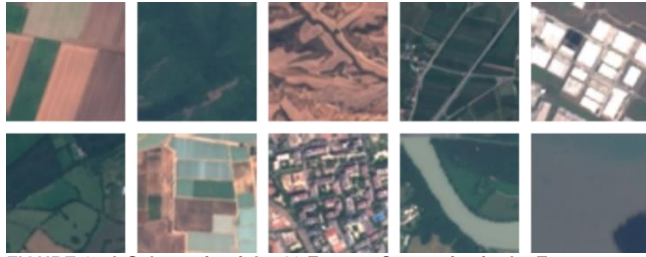


FIGURE 1. A Schematic of the 10 Feature Categories in the Eurosat

2) TEXTURE ANALYSIS

Explaining the complex network modeling procedure for remote sensing images is crucial before beginning texture analysis. A complex network is represented in this modeling approach as a graph $G = \{V, E, W\}$. In this case, V stands for the set of network nodes, which correspond to the set of remote sensing image pixel points shown by $V_i = (x_i, y_i)$. W stands for the weight matrix of the network's edges, and E stands for the set of edges in the network.

This paper measures the distance between pixel locations $P_i(x_i, y_i)$ and $P_j(x_j, y_j)$ using the Euclidean distance, which is computed as follows:

$$D(V_i, V_j) = \sqrt{(x_i - x_j)^2 + (y_i - y_j)^2} \quad (7)$$

The weight of the connected edge is defined as follows [11], assuming that there is a connecting edge between any two-pixel positions:

$$w_{ij} = (x_i - x_j)^2 + (y_i - y_j)^2 + |P_i(x_i, y_i) - P_j(x_j, y_j)| \quad (8)$$

The first rule network can be built based on the provided radius R and weight W and the weight and distance computation formulas. A 64x64 remote sensing image is used as an example, as depicted in Figure 2. Part (b) illustrates the extraction of the image's upper left corner, which has an area measuring 11 by 11 pixels. Part (c) illustrates how, given a radius of $R=3$, the center point is connected to its vertices whose Euclidean distance does not exceed 3. Next, each connecting edge's weight is determined using the weight

formula given the weight parameter $W=2$. Edges having a weight value larger than 2 are removed. The complex network is simplified by keeping just the connecting edges with a weight value of less than 2. Furthermore, the weights are normalized to guarantee that the image's geometric and color information are equally significant. The particular weights are determined in this way:

$$w_{ij} = \frac{(x_i - x_j)^2 + (y_i - y_j)^2 + |P_i(x_i, y_i) - P_j(x_j, y_j)|}{R^2} \quad (9)$$

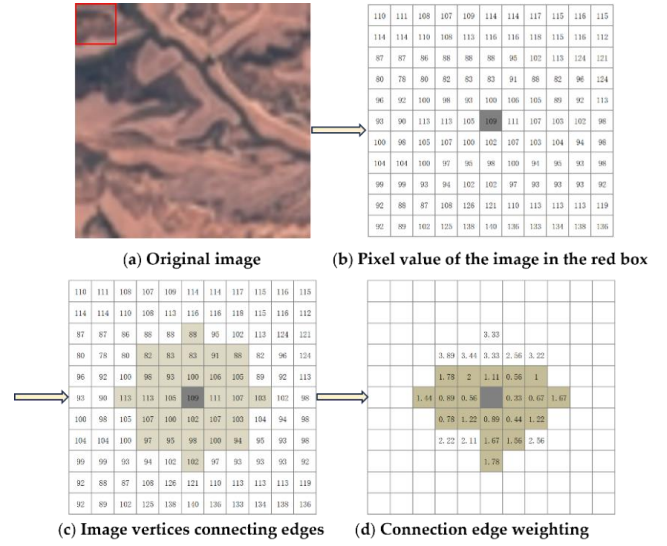


FIGURE 2. Processing of an Image by a Complex Network

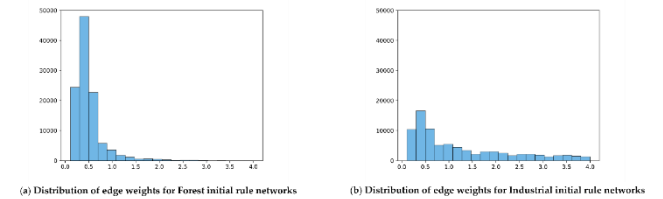


FIGURE 3. Comparison of Edge Weight Distributions in the Initial Rule Network

For instance, the following is the weighting formula between $P(6,5)=105$ and $P(6,6)=109$:

$$w = \frac{(6 - 6)^2 + (5 - 6)^2 + |105 - 109|}{9} = 0.56 \quad (10)$$

Texture classifications in remote sensing images are generally diverse. The Eurosat has ten categories, including Residential Buildings, Industrial Buildings, etc. Distinct texture categories have distinct edge weight distributions of the original rule network, as seen in Figure 3 for the Forest and Industrial. In Figure 3, the distribution of edge weights is more concentrated in the Forest category. It has a smaller mean value, while the distribution of edge weights in the Industrial category is more dispersed and has a higher mean value.

In this paper, we employ the average degree as a metric to explore how the upper limit of the evolution threshold affects

the average degree of ten classes of remote sensing images in the Eurosat. Next, as Figure 4 illustrates, we examine the effective evolution threshold ranges of remote sensing images with various textures. The curves depicted in the figure illustrate the variations in the network's average degree following its initial regular evolution at various evolution thresholds. It is evident that when the evolution threshold approaches its upper bound, the average degree value rises and eventually reaches a steady state. Consequently, the upper threshold significantly influences the effective threshold range, beginning at a lower threshold of 0. When the average degree stabilizes, the network topology mirrors that of the initial regular network, indicating that this evolution threshold is the upper limit of the effective threshold range. To be more precise, the average degree is determined in this way:

$$\text{Average Degree} = \frac{1}{N} \sum_{i=1}^N k_i \quad (11)$$

where N is the total number of nodes in the network and k_i is the degree of node i .

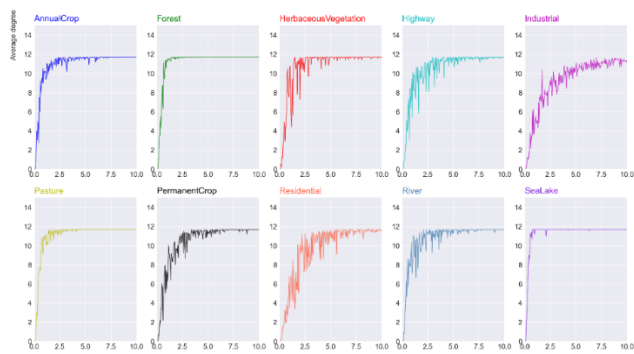


FIGURE 4. Effective Threshold Ranges for Different Texture Images

The remote sensing images of ten distinct texture categories in the figure show variations in the effective evolution threshold range. For instance, the higher evolutionary thresholds of relatively smooth textures, like Forest and Sealake, are smaller, at around 1.65 and 0.8, respectively. However, the upper evolutionary thresholds of somewhat rough textures, like Industrial and Residential, are more significant, at about 11.45 and 7.4, respectively. For other texture categories, the distribution of higher evolutionary thresholds is primarily between 2 and 5. This suggests that the effective threshold range is wide for relatively rough textures and relatively small for relatively smooth textures. In order to increase significantly the classification accuracy of remote sensing images, distinct dynamic threshold evolution methods must be used for images with varying textures. The proper evolution threshold range must be chosen. It should be noted that while the Eurosat is used in this paper as an example, other datasets can employ the same method.

3) ESTABLISHMENT OF COMPLEX NETWORKS

The radius and weight threshold are the two primary parameters in the complex network-building process. After the radius parameter R is chosen, the weight parameter T governs how the network evolves throughout its life cycle, controlling the size of the neighborhood of pixel points. The precise procedure is as follows: in order to determine the pixel average function, each pixel in the image is first treated as a vertex of the complex network. The radius and pixel value information are retrieved by inputting the image. The weight matrix is then built after the weight formula is used to get the weights given the weight threshold and radius threshold. Ultimately, upon normalization, the processed grayscale image is produced. Using the Eurosat as an example, Figure 5 displays the comparison results before and after processing for each category of images, assuming that the weight threshold is $T=2$ and the radius threshold is $R=1$.

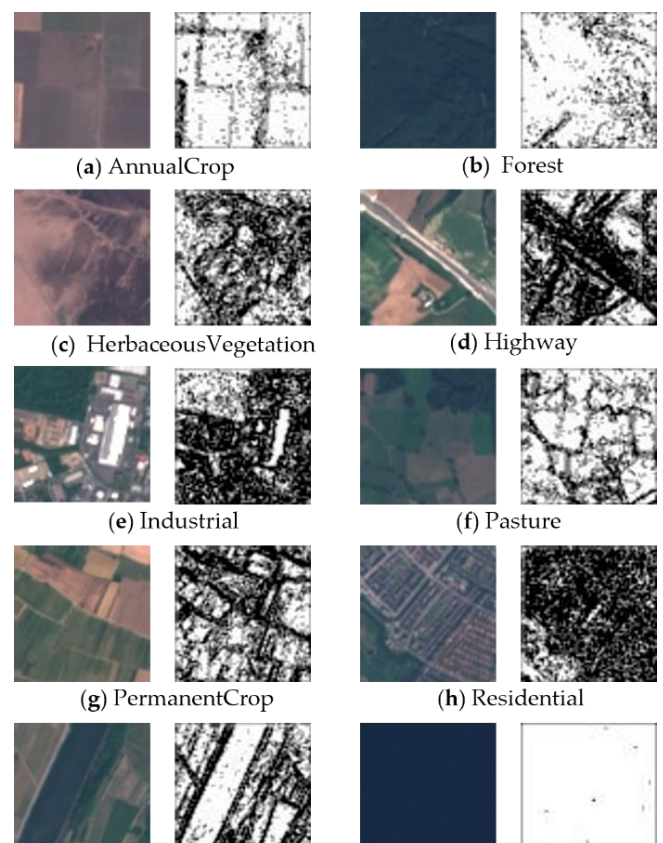


FIGURE 5. Comparison of Images Before and After Complex Networks Processing

The outcomes of setting the weight threshold ($T=2$) and the radius threshold ($R=1$) are displayed in the figure. The grayscale images of the four categories—Annual Crop, Herbaceous Vegetable, Pasture, and River—can better capture the texture characteristics of the category and preserve its original feature information. On the other hand, the four categories—Highway, Industrial, Permanent Crop, and Residential—cannot fully interpret the original image's feature information. Finally, after processing, the two categories—Forest and Sea Lake—lost the original image's feature information. The conclusions established from the texture

study in the preceding section also align with these three relationships: images with varying textures have varying effective evolution threshold ranges.

TABLE 1. Evolution Results of Different Textures at Various Radius Thresholds



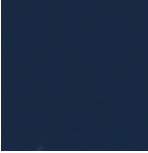


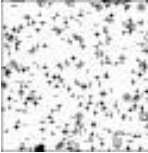












Weight threshold	Industrial	River	SeaLake
T=0 (Original)			
T=1			
T=1.5			
T=2			
T=2.5			
T=3			

Table 1 displays the evolution findings of the three texture classes—River, Industrial, and SeaLake—at various radius thresholds. At T=3, Industrial, which has a more significant effective evolution threshold, does not exhibit substantial feature extraction. On the other hand, River exhibits clear feature information at T=3 and has the second-highest effective evolution threshold. With a reduced effective evolution threshold, SeaLake has nearly no original image feature information at T=3. These findings suggest that, when modeling complex networks on remote sensing images, different categories of images necessitate different effective evolution threshold ranges.

In the preceding section, we observed that various remote sensing images have various evolutionary threshold ranges. Next, using the upper threshold shown in Figure 4, we calculate the weight thresholds for each of the 10 categories. The following table displays the weight threshold T for each category as determined.

TABLE 2. Weight Thresholds for 10 Types of Remote Sensing Images in the EuroSAT

Category	Upper evolutionary threshold	Weight threshold
AnnualCrop	3.85	3.8
Forest	1.65	1.6
HerbaceousVegetation	2.95	2.9
Highway	5.1	5.1
Industrial	11.45	11.4
Pasture	2.7	2.7
PermanentCrop	5.85	5.8
Residential	7.4	7.4
River	4.6	4.6
SeaLake	0.8	0.8

We explore the radius threshold R based on the determined weight thresholds. We first set the threshold $R_0 = 0.5$ and then gradually increase it by 0.5 until reaching the maximum value $R_t = 3$ to allow the complex network to evolve fully. We empirically measured the dataset's classification performance for each set of thresholds to find the ideal radius R. The dataset classification accuracy is maximum at the radius threshold $R = 1.5$, as Table 3 illustrates. As a result, we identified the radius and weight thresholds for every category of remote sensing image in the dataset.

TABLE 3. Determination of Radius Thresholds

Radius threshold	Accuracy
0.5	0.9493
1	0.9496
1.5	0.9522
2	0.9507
2.5	0.9513
3	0.9506

B. Complex Network-Based Prediction for Remote Sensing Image Classification

This paper's experiments were all performed on the AutoDL Arithmetic Cloud Platform using an RTX 3090 graphics card that had been chosen with 24GB of video RAM. The studies used a batch size of 64, a learning rate of 0.001, and a total of 128 training rounds. Classification experiments were conducted on Eurosat images before and after complex network processing using GoogleNet. The model's performance was assessed using the classification accuracy, precision, as well as recall and F1 values.

First, we present the results of processing and classification prediction using weight and radius criteria that are consistent across 10 classes of images in the Eurosa. An 8:2 split of the dataset was made into training and test sets. The original and processed image classification accuracies are displayed in Table 4.

TABLE 4. Image Classification Accuracy under the Same Radius and Weight Thresholds

Group	Radius threshold	Weight threshold	Accuracy
0	0	0	0.9481
1	1	1	0.9520
2	1	1.5	0.9517
3	1	2	0.9489
4	1	2.5	0.9483
5	1	3	0.9519
6	1.5	1	0.9533
7	1.5	1.5	0.9522
8	1.5	2	0.9496
9	1.5	2.5	0.9548
10	1.5	3	0.9498
11	2	1	0.9544
12	2	1.5	0.9539
13	2	2	0.9515
14	2	2.5	0.9498
15	2	3	0.9537
16	2.5	1	0.9533
17	2.5	1.5	0.9504
18	2.5	2	0.9533
19	2.5	2.5	0.9517
20	2.5	3	0.9511
21	3	1	0.9548
22	3	1.5	0.9496
23	3	2	0.9544
24	3	2.5	0.9507
25	3	3	0.9469

Classification prediction of the original image by GoogleNet resulted in a classification accuracy of 0.9481. As shown in Table 4, complex networks with different but consistent radius thresholds and weight thresholds were set to classify the processed images, and the classification accuracy was higher than that of the original image for the first 24 out of 25 groups of experiments. Among them, the highest classification accuracy is 0.9548 when the radius threshold $R=1.5$ and the weight threshold $T=2.5$ and when the radius threshold $R=3$ and the weight threshold $T=1$ are 0.67% higher than that of the original image.

TABLE 5. Image Classification Accuracy, Precision, Recall, and F1-Score under Different Radius and Weight Thresholds

Group	Accuracy	Precision	Recall	F1-score
Original picture	0.7976	0.8030	0.7980	0.7960
After picture	0.7995	0.8040	0.8000	0.7970

The results of applying various weight and radius criteria to the 10 categories of images in the Eurosat are then shown, along with the classification predictions that resulted from this processing. Initially, we split the Eurosat's images into two groups: a training set and a test set, with a ratio of 8:2. Second, we used the 10-fold cross-validation method to assess the model's performance more impartially. The training set data are split into ten sections for this method. The model can be independently trained and verified ten times using one component as the validation set and the other nine parts as the training set in each iteration. Using the training set data to its fullest potential minimizes dependence on a single separation of the training and validation sets. Finally, to confirm the model's ability for generalization, we conducted a last assessment of the cross-validated model using the test set. Table 5 displays the F1 values, recall, precision, and

classification accuracy for the image test set before and after complex network processing. Complex network-processed images perform better than original images in terms of

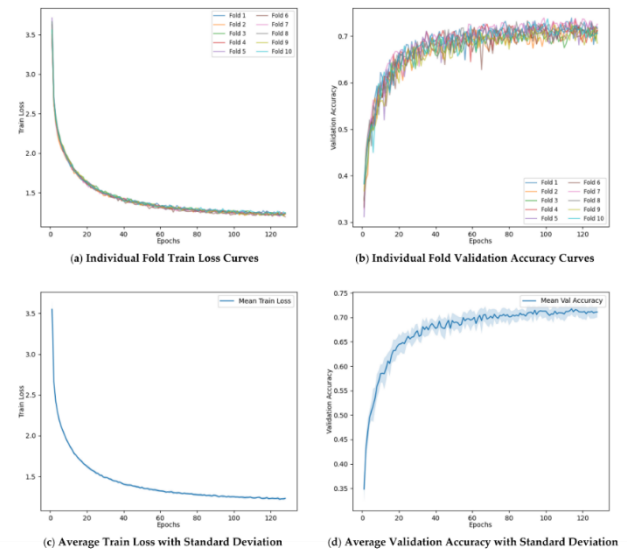


FIGURE 6. Training Loss and Validation Accuracy

accuracy, precision, recall, and F1 value, as Table 5 shows. Notably, the different dataset partition methods account for the discrepancies in accuracy rates between Tables 4 and 5.

The train loss and validation accuracy curves for our model are shown in Figure 6. For clarity's sake, we present four sets of plots: First, part (a) shows how the training loss varies according to the number of training epochs for every fold. All folds' train loss curves show a steady decline that levels off at about 120 epochs, suggesting that the model's loss gradually drops and approaches a converged state. This implies no overfitting symptoms, and the model learns features across all folds efficiently. Part (b) compares how each fold's validation accuracy changes throughout epochs. The validation accuracy curves demonstrate the model's excellent accuracy (about 0.7) for each fold, which validates the model's capacity for generalization. Finally, the average training loss and average validation accuracy for all folds are displayed in parts (c) and (d), respectively, and are shaded to represent the standard deviation.

In summary, the classification performance of the images from the Eurosat is much enhanced by using complex network processing. The gains in accuracy, precision, recall, F1 values demonstrate the success of our approach. These results demonstrate the ability of complex network processing to improve image classification tasks, which can be used for various satellite imagery analysis and remote sensing applications.

IV. Discussion

In this paper, we combine complex networks and deep learning to enhance the recognition and classification of remote sensing images based on their texture features. By constructing a network that connects image pixels, we

effectively capture patterns and structures within the images, thereby improving classification accuracy and performance. This paper proposes a complex network-based method for remote sensing image recognition and categorization. Different characteristics of diverse settings are initially studied by analyzing remote sensing images with varying textures. According to the paper, images with coarser textures in categories including residential, highway, industrial, and permanent crop require higher thresholds for evolution. On the other hand, images in the Forest and SeaLake categories require lower thresholds due to their softer textures. Furthermore, categories with intermediate threshold values for evolution, like AnnualCrop, HerbaceousVegetation, Pasture, and River, have rougher textures. Secondly, we integrate static statistics and threshold evolution from complex networks to extract features from remote sensing images depicting diverse textures in various scenes. The convolutional neural network GoogleNet is then employed to categorize and predict images processed with a range of weight and radius thresholds, and the outcomes are compared to those derived from the original images. The experimental results show that our suggested approach achieves high accuracy rates, providing new understandings of the prediction and classification of remote sensing images.

One limitation of this paper is the reliance on the Eurosat, which may not generalize to other image datasets. Future research should explore the application of this method to diverse datasets to validate its robustness and versatility. Additionally, in experiments with the Eurosat, remote sensing images featuring diverse textures are differentiated only by varying weight thresholds, while radius thresholds remain consistent. Further optimization of the radius and weight thresholds could be explored to achieve better performance.

REFERENCES

- [1] G. Cheng, J. Han, and X. Lu, "Remote sensing image scene classification: Benchmark and state of the art," *Proc. IEEE*, vol. 105, no. 10, pp. 1865–1883, Oct. 2017.
- [2] W. Li, et al., "Deep learning based oil palm tree detection and counting for high-resolution remote sensing images," *Remote Sens.*, vol. 9, no. 1, pp. 22, Jan. 2016.
- [3] Z. Ma, et al., "Satellite imagery classification based on deep convolution network," *Int. J. Comput. Inf. Eng.*, vol. 10, no. 6, pp. 1155–1159, Jun. 2016.
- [4] Z. Zhou, Y. Zheng, H. Ye, et al. (2018, September). Satellite image scene classification via convnet with context aggregation. presented at PCM 2018: 19th Pacific-Rim Conference on Multimedia, Hefei, China, September 21–22, 2018, Proceedings, Part II.
- [5] X. Sun, Q. Zhu, and Q. Qin, "A multi-level convolution pyramid semantic fusion framework for high-resolution remote sensing image scene classification and annotation," *IEEE Access*, vol. 9, pp. 18195–18208, 2021.
- [6] R. Fan, et al. (2019, July). Attention based residual network for high-resolution remote sensing imagery scene classification. presented at IGARSS 2019-2019 IEEE International Geoscience and Remote Sensing Symposium.
- [7] Q. Liu, et al., "DeepSat v2: feature augmented convolutional neural nets for satellite image classification," *Remote Sens. Lett.*, vol. 11, no. 2, pp. 156–165, Feb. 2020.
- [8] A. R. Backes, D. Casanova, and O. M. Bruno, "A complex network-based approach for boundary shape analysis," *Pattern Recognit.*, vol. 42, no. 1, pp. 54–67, Jan. 2009.
- [9] W.N. Gonçalves, J.A. Silva, and O.M. Bruno. (2010, November). A rotation invariant face recognition method based on complex network. presented at CIARP 2010: 15th Iberoamerican Congress on Pattern Recognition.
- [10] L. Zhou, et al., "Hierarchical palmprint feature extraction and recognition based on multi-wavelets and complex network," *IET Image Process.*, vol. 12, no. 6, pp. 985–992, Jun. 2018.
- [11] Z. Ma and G. Huang, "Image recognition and analysis: A complex network-based approach," *IEEE Access*, vol. 10, pp. 109537–109543, 2022.
- [12] R. M. D'Souza, M. di Bernardo, and Y.-Y. Liu, "Controlling complex networks with complex nodes," *Nat. Rev. Phys.*, vol. 5, no. 4, pp. 250–262, Apr. 2023.
- [13] P. Erdős and A. Rényi, "On random graphs I," *Publ. Math. Debrecen*, vol. 6, pp. 290–297, 1959.
- [14] D. J. Watts and S. H. Strogatz, "Collective dynamics of 'small-world' networks," *Nature*, vol. 393, no. 6684, pp. 440–442, Jun. 1998.
- [15] R. Ding, et al., "Application of complex networks theory in urban traffic network researches," *Netw. Spat. Econ.*, vol. 19, pp. 1281–1317, 2019.
- [16] P. Helber, et al., "Eurosat: A novel dataset and deep learning benchmark for land use and land cover classification," *IEEE J. Sel. Top. Appl. Earth Obs. Remote Sens.*, vol. 12, no. 7, pp. 2217–2226, Jul. 2019.
- [17] Z. Liu and Y. Qiao, "Adaptive Evolution Threshold for Multiscale Dynamic Texture Classification Based on Complex Network," in *Advances in Intelligent Information Hiding and Multimedia Signal Processing: Proceeding of the IIH-MSP 2021 & FITAT 2021*, Kaohsiung, Taiwan, Volume 1, Singapore: Springer Nature Singapore, 2022, pp. 203–213.



YUCHEN WANG, born in 2000, from Luoyang, Henan, China. She is currently a second-year graduate student at China University of Geosciences, Beijing. Her research interests include image recognition and processing, machine learning, and deep learning.



GUANGDONG HUANG is currently the Ph.D. Associate Professor of mathematics with the School of Science, China University of Geosciences, Beijing, China. He has published more than 20 research papers independently or cooperatively, and presided over and participated in nine projects. His research interests include mathematical modeling, modern intelligent algorithm, financial engineering, and probability theory and statistics. He is mainly engaged in the research and teaching of applied statistics and machine learning.



ZONGWEI WANG, male, was born in Suzhou, Anhui in 1988. He is a graduate student and is now a senior engineer. He is mainly engaged in satellite remote sensing application research.